Article ID: 1671-3664(2005)02-0251-14

Earthquake safety assessment of concrete arch and gravity dams

Lin Gao (林皋)† and Hu Zhiqiang ‡(胡志强)‡

School of Civil and Hydraulic Engineering, Dalian University of Technology, Dalian 116024, China

Abstract: Based on research studies currently being carried out at Dalian University of Technology, some important aspects for the earthquake safety assessment of concrete dams are reviewed and discussed. First, the rate-dependent behavior of concrete subjected to earthquake loading is examined, emphasizing the properties of concrete under cyclic and biaxial loading conditions. Second, a modified four-parameter Hsieh-Ting-Chen viscoplastic consistency model is developed to simulate the rate-dependent behavior of concrete. The earthquake response of a 278m high arch dam is analyzed, and the results show that the strain-rate effects become noticeable in the inelastic range. Third, a more accurate non-smooth Newton algorithm for the solution of three-dimensional frictional contact problems is developed to study the joint opening effects of arch dams during strong earthquakes. Such effects on two nearly 300m high arch dams have been studied. It was found that the canyon shape has great influence on the magnitude and distribution of the joint opening along the dam axis. Fourth, the scaled boundary finite element method presented by Song and Wolf is employed to study the dam-reservoir-foundation interaction effects of concrete dams. Particular emphases were placed on the variation of foundation stiffness and the anisotropic behavior of the foundation material on the dynamic response of concrete dams. Finally, nonlinear modeling of concrete to study the damage evolution of concrete dams during strong earthquakes is discussed. An elastic-damage mechanics approach for damage prediction of concrete gravity dams is described as an example. These findings are helpful in understanding the dynamic behavior of concrete dams and promoting the improvement of seismic safety assessment methods.

Keywords: arch dam; gravity dam; earthquake safety; dynamic behavior of concrete; strain-rate effect; joint-opening effect; dam-foundation interaction; non-linear modeling

1 Introduction

Many large concrete arch dams and roller-compacted concrete gravity dams are being built in highly seismic areas of China. In fact, some may be among the highest arch or roller-compacted concrete dams in the world. The capability of these dams to resist earthquake forces is of great concern.

In current practice, earthquake resistant design of concrete dams is carried out on the basis of linear elastic analyses and the allowable stress concept. Due to the large uncertainties in predicting future earthquake ground motions and a lack of understanding of the performance of concrete dams under strong earthquakes, the adopted design levels in different countries are quite diversified (Lin *et al.*, 2003). In addition, the key property that determines the capacity of concrete dams to withstand earthquakes is the allowable tensile strength of the material, which is still an open issue, and therefore a widely accepted standard is not available. As a result, the seismic safety of concrete dams is assessed based on the engineering judgment and other considerations by experts. To improve the earthquake resistant design of concrete dams, some aspects which are essential for seismic safety assessment are reviewed and discussed in the following paragraphs. This problem has been the subject of numerous investigations in the past twenty years (Fenves *et al*., 1992; Hall, 1998; Villiappan *et al.*, 1999; Liu *et al*., 2002; Du and Wang, 2004). No attempt is made here to give a general review of the vast literature in this field; rather this paper focuses on research currently being carried out at Dalian University of Technology, China.

2 Dynamic properties of concrete

Most studies have shown that concrete is sensitive to the rate of loading (Bischoff and Perry, 1991; Malvar and Ross, 1998). The material strength, stiffness and ductility (or brittleness) are rate-dependent. However, the great majority of experimental results in the literature were restricted to uniaxial and monotonic loading conditions. In order to obtain a better understanding of concrete behavior subjected to earthquake loading, dynamic experiments on concrete specimens were performed in the laboratory of Dalian University of Technology.

Correspondence to: Lin Gao, School of Civil and Hydraulic Engineering, Dalian University of Technology, Dalian 116024, China
Tel: 86-411-84708952; Fax: 86-411-84708501
E-mail: gaolin@dlut.edu.cn
†Professor; ‡Doctor, Lecturer

Supported by: National Natural Science Foundation of China Under Grant No.50139010
Received 2005-11-24; **Accepted** 2005-12-20

2.1 Cyclic loading effect (Yan *et al*., 2005)

Earthquake load is characterized by its cyclic behavior with varying amplitude. To study such an effect, 76 concrete specimens were tested on the MTS810 electro-fluid servo-universal machine at Dalian University of Technology to investigate the effect of initial static load, frequency and rate of amplitude increment of cyclic loading on the dynamic properties of concrete. The applied load pattern is shown in Fig.1.

$$F = A\sin(2\pi ft) + F_0 \tag{1}$$

where F_0 is the initial static loading; A is the varying amplitude and f is the cyclic frequency.

As $\sigma = E\varepsilon$, the expression of strain rate is

$$\frac{\mathrm{d}\varepsilon}{\mathrm{d}t} = \frac{1}{E}\left(\frac{\mathrm{d}\sigma}{\mathrm{d}t} - \frac{\sigma}{E}\frac{dE}{dt}\right) \approx \frac{1}{E}\frac{\mathrm{d}\sigma}{\mathrm{d}t} = \frac{1}{ES}\frac{\mathrm{d}F}{\mathrm{d}t} \tag{2}$$

where E is the elastic modulus and S is the cross section area of the specimen. It is observed that the variation of E with time is fairly slight, and the second term of Eq. (2) can be neglected. Substituting Eq. (1) into (2), it is seen that the strain rate effects consist of two parts ε_1 and ε_2, the phase difference between them is 90 and the former is dominant.

$$\frac{\mathrm{d}\varepsilon}{\mathrm{d}t} = \dot{\varepsilon}_1 + \dot{\varepsilon}_2 = \frac{1}{ES}\left[2\pi fA\cos(2\pi ft) + \frac{\mathrm{d}A}{\mathrm{d}t}\sin(2\pi ft)\right] \tag{3}$$

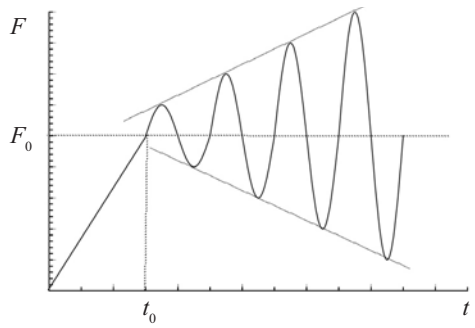

Fig. 1 Applied load pattern

where $\mathrm{d}A/\mathrm{d}t = \Delta A \cdot f$, ΔA is the increment of amplitude per cycle. Eq.(3) clearly shows that the dynamic strength of concrete subjected to variable amplitude cyclic loading is mainly determined by the maximum loading rate of the individual cycle $\dot{\varepsilon}_1$, and the effect of the rate of amplitude increment $\dot{\varepsilon}_2$ is insignificant. Hence, the dynamic strength of concrete under cyclic loading conditions can be predicted from the monotonic loading conditions. The tested tensile strength of concrete under monotonical loading condition is given in Table 1. The results obtained under cyclic loading conditions are given in Table 2, where σ_{cp} is the average tensile strength measured by cyclic loading test and $\sigma \pm \Delta\sigma$ is the predicted tensile strength calculated from the result of monotonic loading test (σ is the mean value, and $\Delta\sigma$ is the standard deviation).

The magnitude of the initial static loading F_0 affects the strength of the concrete under cyclic loading conditions, which is limited because the specimens need to remain in tension, thus reducing the possible range of initial static loading (see Fig.1). It is seen that as the initial static load increases, the dynamic strength of concrete decreases.

The experimental results also show that as the number of cycles increase, micro-cracks in the specimen develop, and eventually the irreversible deformation of concrete also increases.

2.2 Biaxial compressive behavior of concrete

Dynamic compressive tests of 71 cubic specimens were conducted on the electro-fluid multi-axial test machine at Dalian University of Technology. The lateral pressure was kept in proportion with the load acting in the main direction with the ratios of 0, 0.25, 0.5, 0.75 and 1. The test results are listed in Table 4.

The hybrid effect of the strain rate and lateral restrained pressure may be expressed as follows:

$$\frac{f_c}{f_s} = k_1 + k_2\log\left(\frac{\dot{\varepsilon}_c}{\dot{\varepsilon}_s}\right) + \frac{k_3}{(1+\alpha)^2} + \frac{k_4\alpha}{(1+\alpha)^2}$$

where the fitted experimental constants of k_1, k_2, k_3 and k_4 are −0.446, 0.08745, 6.42 and 1.433, respectively,

Table 1 Tensile strength of concrete under monotonic loading conditions

No	Loading rate (MPa/s)					
	10^{-5}	10^{-4}	10^{-3}	10^{-2}	10^{-1}	$10^{-0.3}$
1	1.97	2.18	2.81	2.88	3.53	3.88
2	2.24	2.52	2.94	2.72	3.70	4.23
3	2.39	2.47	2.62	3.25	3.06	3.67
4	2.44			2.72	3.33	
5	1.98			2.77		
6				2.89		
σ	2.21	2.39	2.79	2.87	3.40	3.93
$\Delta\sigma$	0.198	0.15	0.131	0.183	0.238	0.231

Table 2 Tensile strength of concrete under cyclic loading conditions

Pre-load F_0(MPa)	Frequency f(Hz)	Increment amplitude (MPa)	Measured strength σ_{cp} (MPa)	$\dot{\varepsilon}_1$ (10^{-4}/s)	$\dot{\varepsilon}_2$ (10^{-6}/s)	Predicted strength σ±Δσ(MPa)
1.6	0.5	0.08	2.49	0.943	1.35	2.38±0.153
	2	0.08	2.74	4.39	4.86	2.54±0.143
	10	0.08	2.88	27.3	27.1	2.81±0.141
	20	0.08	2.86	54.1	54.7	2.83±0.156
	30	0.08	2.87	82.5	82.7	2.85±0.173
1.6	2	0.016	2.49	3.40	0.96	2.38±0.145
	2	0.034	2.82	4.65	2.07	2.55±0.152
	2	0.08	2.74	4.35	4.86	2.54±0.150
	2	0.32	2.73	4.31	19.4	2.54±0.150
2.0	2	0.08	2.51	1.95	4.86	2.43±0.136

Table 3 Effect of magnitude of initial static loading on the cyclic dynamic strength of concrete (frequency of cyclic loading 2Hz, amplitude increment per cycle ΔA=0.08 MPa)

Initial static loading F_0	Dynamic strength (average) (MPa)
1.6 MPa (72.4% f_c)	2.75, 2.73, 2.79, 2.70 (2.74)
2.00 MPa(90.5% f_c)	2.43, 2.61, 2.50 (2.51)

Table 4 Strain rate effects on the biaxial strength of concrete MPa

Strain rate(1/s)	No.	Load ratio（σ_1：σ_2）				
		1：0	1：0.25	1：0.5	1：0.75	1：1
10^{-5}	1	9.93	15.61	16.08	16.46	14.16
	2	9.67	14.34	15.85	17.03	13.48
	3	9.93	14.64	16.03	15.92	14.37
	4	9.83		16.55	16.15	
	Average	9.84	14.86	16.13	16.39	14.00
10^{-4}	1	10.59	15.28	17.35	17.20	16.07
	2	10.76	15.77	16.40	16.60	14.49
	3	10.52	15.38	16.29	16.46	16.05
	4	10.66		16.66		14.65
	Average	10.63	15.48	16.68	16.75	15.32
10^{-3}	1	11.75	15.66	17.68	17.85	17.40
	2	11.14	16.18	17.21	17.40	16.42
	3	11.25	16.67	17.19	17.97	15.61
	4	11.38			16.94	17.22
	Average	11.38	16.17	17.36	17.54	16.66
10^{-2}	1	12.78	17.30	17.66	18.08	18.00
	2	12.04	16.93	18.23	19.50	17.79
	3	12.15	17.23	19.17	19.62	18.23
	4			17.89	17.44	
	Average	12.32	17.15	18.24	18.66	18.01

the coefficient of correlation is 0.9580; f_c is the biaxial compressive strength of concrete corresponding to a given strain rate; f_s is the static uniaxial axial compressive strength of concrete; and α is the lateral load ratio $\alpha=\sigma_2/\sigma_1$.

The stress-strain curves for different load ratios are shown in Fig.2.

3 Strain-rate effects

Since the material properties of concrete dams are rate-dependent, when they are subjected to earthquake excitations, the stress-strain relationships exhibited in different parts of the dam will vary depending on the strain-rate it experienced. However, the effect of rate-

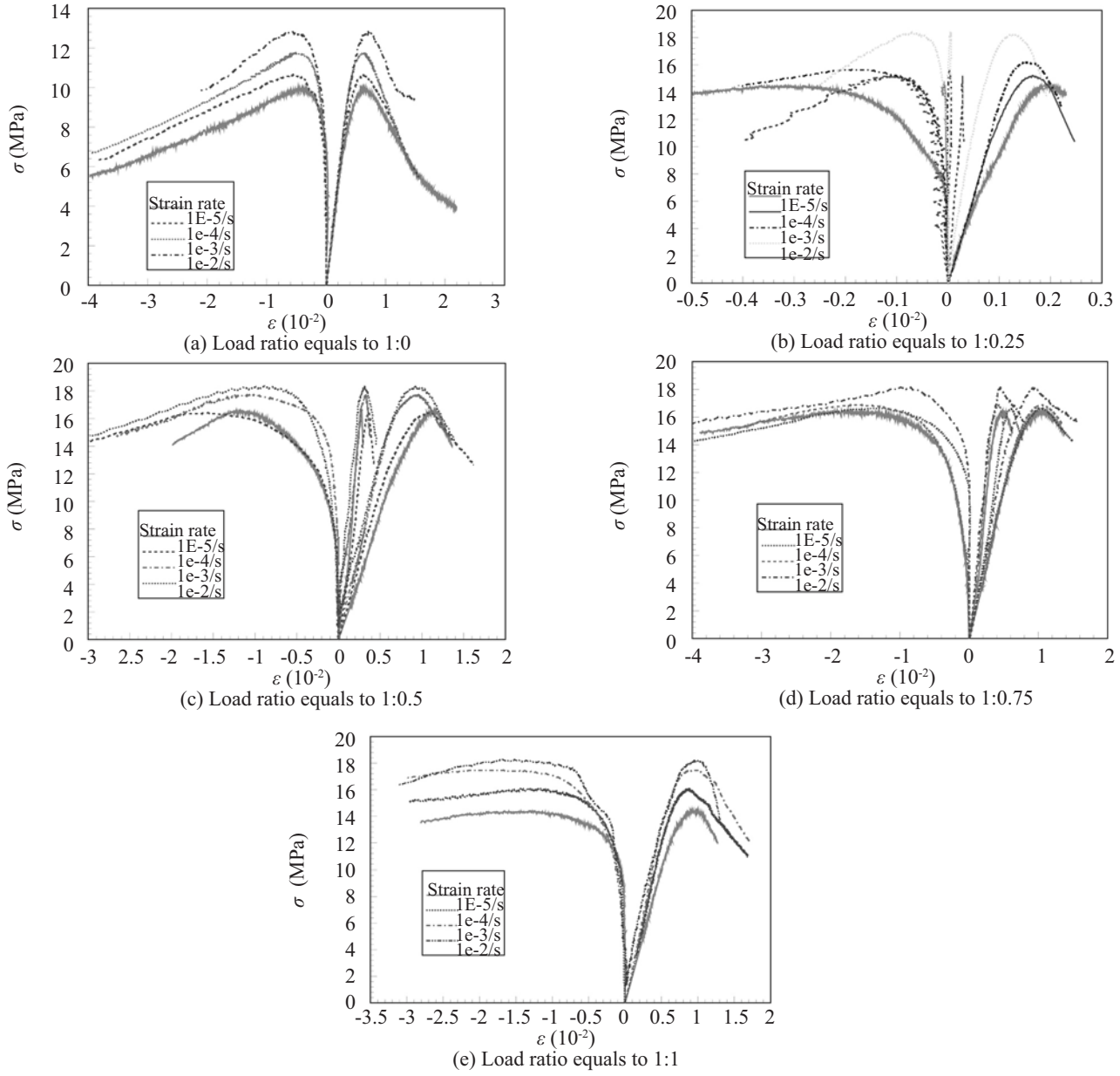

(a) Load ratio equals to 1:0

(b) Load ratio equals to 1:0.25

(c) Load ratio equals to 1:0.5

(d) Load ratio equals to 1:0.75

(e) Load ratio equals to 1:1

Fig. 2 Stress-strain curves for different load ratios

sensitivity on the earthquake response of concrete dams has not been well established and is not fully understood. In conventional design practice, this effect is estimated basing on simplified assumptions. That is, for a wide variety of dam structures, the material properties and the earthquake excitation level, in all cases the dynamic strength of concrete is increased by, say, 30% of the value specified for static case.

Based on the concept of a consistent viscoplastic model, a modified four-parameter Hsieh-Ting-Chen model was developed by the authors to investigate the strain rate effects on the seismic response of concrete dams(Lin and Xiao, 2002). In this model, it is assumed that during viscoplastic flow, the actual stress state remains on the yield surface and satisfies the consistency condition, so that the yield surface is rate-dependent and can change its size and shape according to the value of the viscoplastic strain rate. In addition, two internal variables corresponding to compression and tension, respectively, are introduced, thereby allowing the hardening/softening behavior in compression and tension to be described separately.

A 278 m high Xiluodu arch dam subjected to earthquake excitation is analyzed by the proposed model. The material properties for the study are as follows: for the dam body E=2.4×10^{4}MPa, ν=0.17, ρ=2.4×10^{3}kg/m^3, static compressive strength f_c=30MPa, and static tensile strength f_t=2.5MPa; for the foundation rock E=1.6×10^{4}MPa, ν=0.25, ρ=2.0×10^{3}kg/m^3. The damping ratio of the dam and the foundation equals 0.05. The dam and the foundation are discretized into 450 and 1040 iso-parametric elements, respectively. Figure 3 shows the discretized dam-foundation system. The design earthquake acceleration is 0.321g. Figure 4 shows the

normalized time histories of the input motion.

The calculated stress-strain relationships for uniaxial compression and uniaxial tension by using this model are shown in Fig.5. Fairly good agreement between the calculated results and the experimental data is achieved. The strain-rate dependency mainly affects the inelastic range of the stress-strain curve.

Three response analyses for the dam were performed including: an elastic analysis, a rate-independent plastic analysis and a rate dependent viscoplastic analysis. In the numerical calculation, the static water pressure, the gravitational load and the earthquake load are all included. The maximum values of the first and the third principle stresses in the dam for a full reservoir are shown in Table 5, and the principle stress distributions are shown in Fig. 6. It is seen that rate-dependency behavior does not affect the compressive stresses, but becomes noticeable for tensile stresses. This phenomena can be physically explained with the help of Fig.5. It is clearly shown that in the low stress range, the stress-strain relationship is not sensitive to the strain rate. However, as it approaches the peak stress range, the strain rate effect becomes more noticeable. Usually, an arch dam has a large safety factor in compression of about 4.0, and the structure mainly exists in the low stress range, which is why strain-dependency does not significantly influence the compressive stress response. However, for the tensile stress response, which plays a predominant role in the safety evaluation of the dam structure, the effect of rate-dependency is apparent.

4 Modeling of joint-opening effects of arch dams

The damage to the Pacoima arch dam during the 1971 San Fernando and 1994 Northridge earthquakes provides evidence that the contraction joints of arch dams tend to open during strong seismic events. The weakening of dam integrity and possible damage to joint waterstops raised a safety concern to engineers when these joint openings become significant. Since

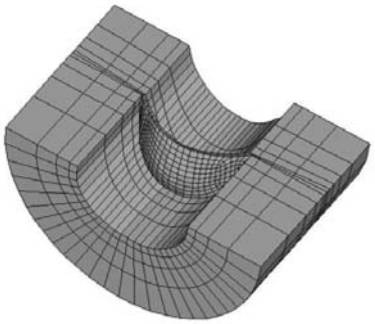

Fig. 3 Geometry and mesh of arch dam

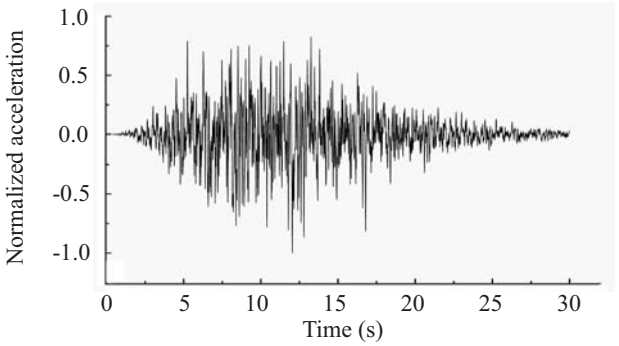

Fig. 4 Time histories of earthquake input

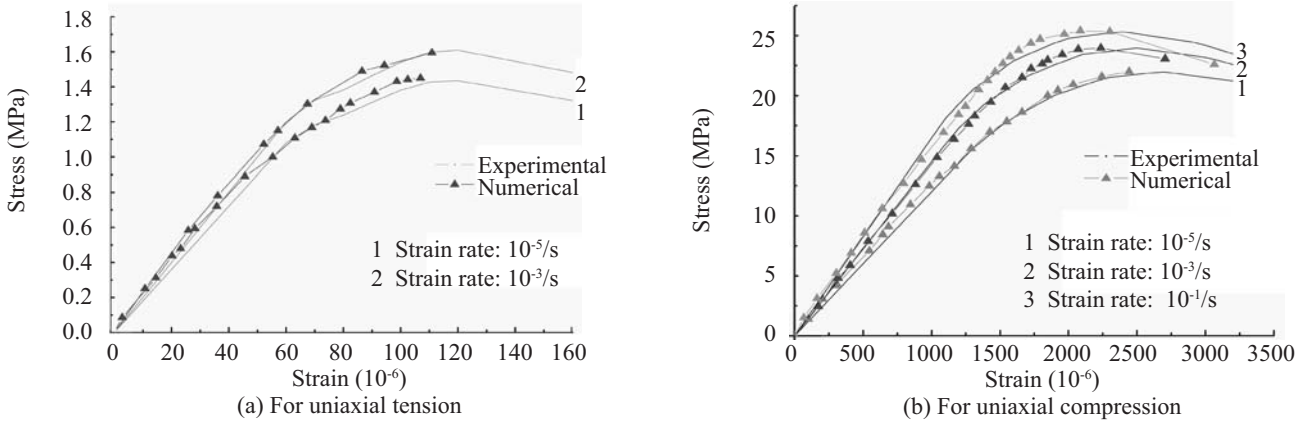

(a) For uniaxial tension (b) For uniaxial compression

Fig. 5 Stress-strain relationship of model under different strain rates

Table 5 Maximum seismic stresses of arch dam

Model	Compression (MPa)	Tension (MPa)
Elastic	-12.15	5.80
Rate independent plastic	-13.15	3.46
Rate dependent viscoplastic	-13.10	4.48

early 1980 s, many studies have been carried out on behaviors of such joints and their effect on the earthquake response of arch dams (Fenves *et al*., 1992; Zhang *et al*., 2000; Du *et al*., 2000). A large number of algorithms for the numerical solution of this problem have been developed. As this is a kind of frictional contact problem characterized by a highly nonlinear nature, which is still under development, considerable discrepancies have been found from the results predicted by various algorithms concerning the magnitude and the distribution of the joint opening along the dam axis. In order to obtain a better understanding of the joint-opening phenomenon, a non-smooth Newton algorithm was developed by the authors to deal with this problem (Lin *et al*, 2004). In the proposed approach, the contact conditions are reformulated as nonlinear complementary equations and further replaced by their equivalent set of non-smooth equations for ease of numerical calculation. The final equations are solved by a generalized damped Newton method. This approach has the advantage of global convergence.

The earthquake response of two high arch dams currently under construction in southwest China is analyzed and compared. The first is the 278 m high Xiluodu arch dam, which is located in a U-shaped canyon. The structure and its foundation were discretized into 99,507 finite elements (107,662 nodes in case of zero joint) as shown in Fig.7. The acceleration time histories of the Koyna earthquake with three-components were chosen as the input motion. The maximum horizontal acceleration is 0.321g. The earthquake waves excited vertically upward from the bottom of the model. Cases with 0, 3, 5, 7, 9, 11 and 13 contraction joints were studied (13 joints has 608 pairs of contact nodes). The arrangement of contraction joints along the dam axis is shown in Fig.8.

In the calculation, the dead weight of the dam and the reservoir water pressure are included and the low operating water level (70 m below the dam crest) is used for the analyses. This reservoir condition is regarded as the most unfavorable case for a joint opening. Opening and sliding of the joints is allowed. The frictional coefficient between the contact concrete faces is assigned as 1.0. Cases where sliding is not allowed due to keying action produced by shear keys are also calculated and compared. The maximum joint opening in the normal

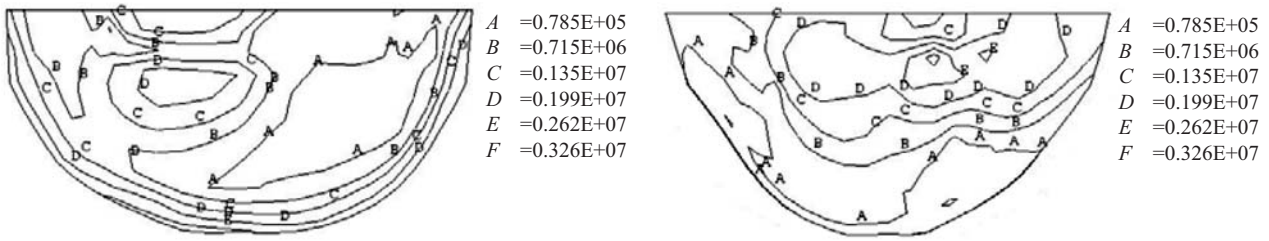

(a) First principle stresses

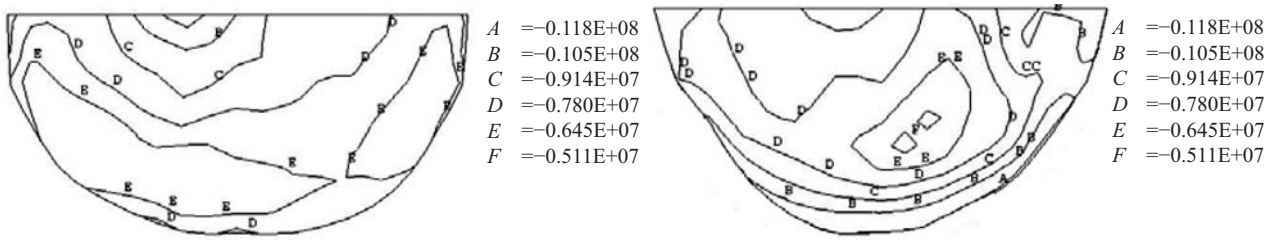

(b) Third principle stresses

Fig. 6 Distribution of principle stresses (upstream and downstream face) - rate dependent viscoplastic model (high reservoir water level) (Pa)

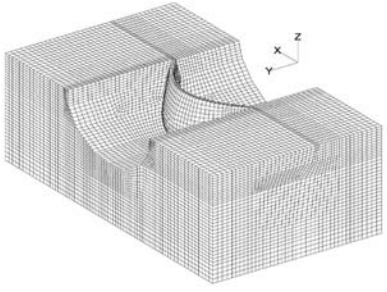

Fig. 7 FEM model of dam-foundation system of Xiluodu arch dam

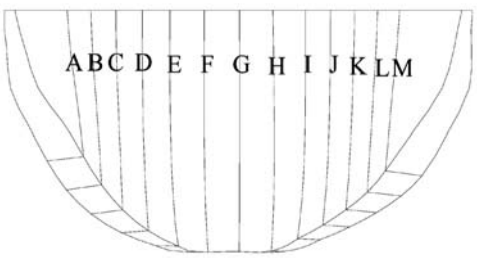

Fig. 8 Arrangement of contraction joints of Xiluodu arch dam (downstream view)

direction and maximum joint sliding in the tangential direction are shown in Tables 6 and 7, respectively.

Figure 9 shows envelops of maximum major principle stresses (tension) and maximum minor principle stresses (compression) with and without joints, respectively.

The second example is the 292 m high Xiaowan arch dam built in a relatively wide V-shaped canyon. Material properties of the dam and foundation are: E_d=21 GPa, ρ_d=2400 kg/m^3, v_d=0.18; E_f=21 GPa; ρ_f=2000kg/m^3, v_f=0.25. The reservoir water level is 59 m below the dam crest. The same Koyna record is used as the input motion. The maximum design acceleration is 0.308 g. The model is discretized into 117,842 finite elements

Table 6 Comparison of maximum joint opening in the normal direction

cm

Case		A	B	C	D	E	F	G	H	I	J	K	L	M
3 joints	U				1.2318			1.1872			0.9514			
	D				1.4765			1.1081			0.2694			
5 joints	U	2.2857			1.3983			0.8804			0.7988			2.6609
	D	2.5471			1.6225			0.8188			0.3918			2.7465
7 joints	U	1.9256		1.3610		1.3857		0.6824		0.4410		1.4104		2.0125
	D	2.0796		1.3526		1.4523		0.6011		0.3441		1.1652		2.2459
9 joints	U	1.9363		1.2165		1.0609	0.5573	0.2906	0.2351	0.5318		1.2668		2.0778
	D	2.0649		1.1473		1.1349	0.6132	0.2980	0.2209	0.4720		1.0562		2.3106
11 joints	U	1.9018		1.1104	0.542	0.8410	0.5666	0.2928	0.2255	0.3346	0.6738	0.9305		1.943
	D	2.0495		1.1437	0.6783	0.9365	0.6245	0.2985	0.2128	0.3405	0.4768	0.7093		2.1777
13 joints	U	1.0587	0.8459	0.8185	0.5636	1.1205	0.6770	0.3060	0.2006	0.3162	0.7346	1.1573	0.9524	1.1037
	D	1.2152	0.8189	0.9206	0.7635	1.2656	0.7346	0.3277	0.2043	0.2467	0.5412	1.0896	0.8093	1.4153
7 joints*	U	0.1995		0.3032		0.3533		0.6824		0.3424		0.3157		0.5273
	D	0		0.1809		0.3411		0.7538		0.3721		0.2555		0.3696

Note: U-upstream face; D-downstream face; * Earthquake wave excites only in river direction

Table 7 Comparison of maximum joint sliding in tangential direction

cm

Case		A	B	C	D	E	F	G	H	I	J	K	L	M
3 joints	U				1.6279			2.2801			1.1519			
	D				1.635			2.3538			1.2571			
5 joints	U	5.2639			0.9770			2.2869			0.9593			6.1362
	D	5.2561			1.0141			2.4563			1.0149			6.1421
7 joints	U	4.4157		2.0193		1.4365		1.2754		0.6662		1.1794		5.6925
	D	4.3995		2.0009		1.4851		1.1155		0.6209		1.2164		5.5829
9 joints	U	4.1929		1.9487		1.1633	0.8888	0.7064	0.5710	0.7005		1.1887		6.3588
	D	4.155		1.9496		1.3075	0.9639	0.7755	0.5725	0.7563		1.2148		6.3708
11 joints	U	4.1036		1.9933	0.9019	0.7266	0.8654	0.6153	0.5297	0.5176	0.7967	1.1619		5.7318
	D	4.1079		2.0032	0.9278	0.8354	0.9337	0.6858	0.5323	0.5720	0.8444	1.1662		5.7218
13 joints	U	3.1199	1.9591	1.7862	1.2317	0.9936	0.8463	0.5493	0.4662	0.4176	0.5654	0.8908	2.5212	3.8773
	D	3.1231	1.8984	1.8168	1.2678	1.1039	0.6015	0.5777	0.4637	0.4567	0.6525	0.9593	2.5066	3.6791
7 joints*	U	0.4088		0.7680		0.4444		0.1022		0.5141		0.5036		2.4088
	D	0.2949		0.7958		0.4837		0.1092		0.5489		0.5332		2.2744

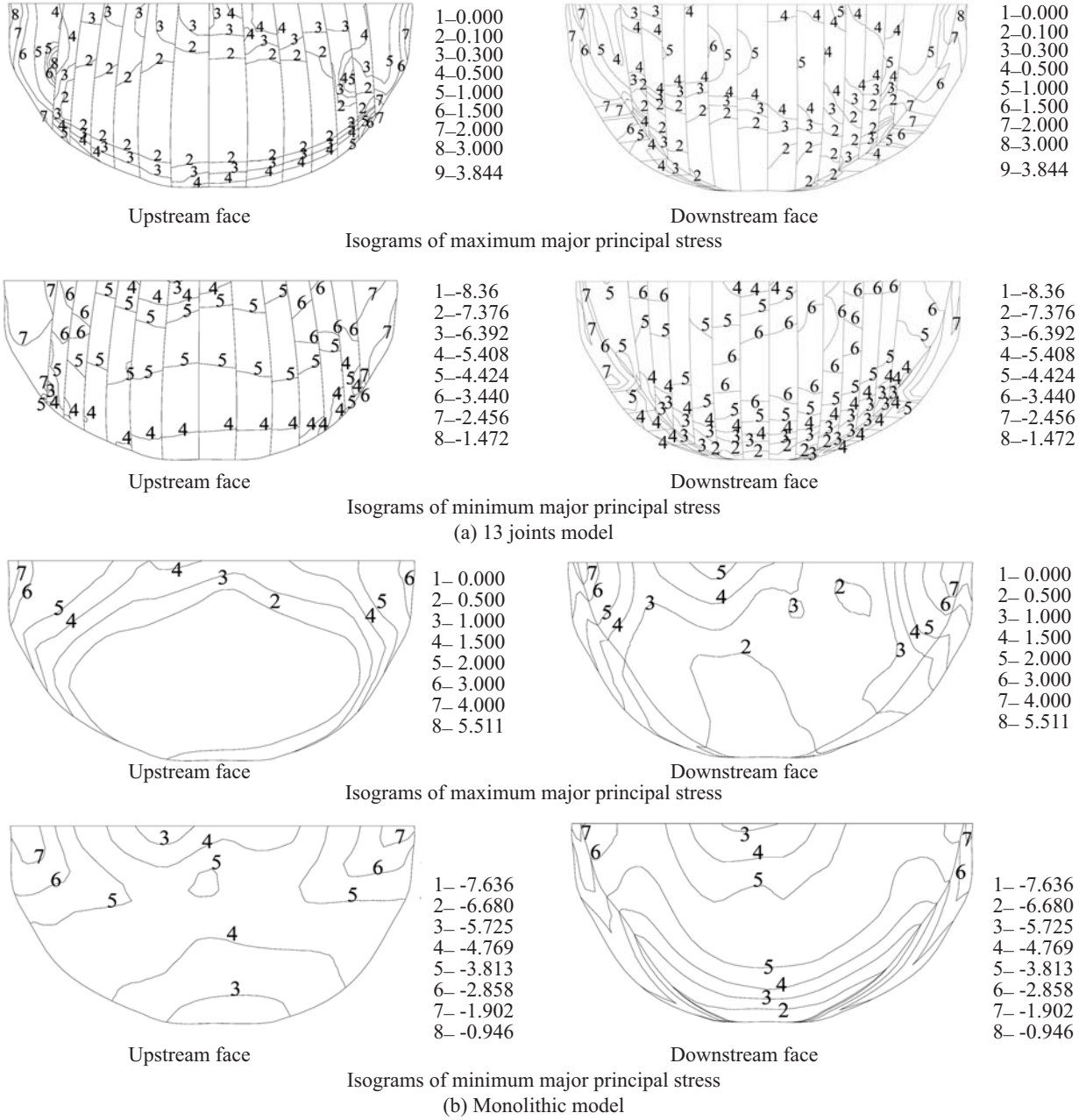

Fig. 9 Isograms of maximum and minimum major principal stresses for 13 joint & monolithic models (MPa)

(126,979 nodes in case of zero joint). Cases with 0, 3, 5, 9, and 11 joints were analyzed. The FEM model and the arrangement of contraction joints are shown in Figs.10 and 11, respectively. For comparison, a five-joint model where joint sliding is prevented by the keying action was also analyzed. Tables 8 and 9 show the maximum joint opening and sliding along the dam axis, respectively.

These results lead to the following conclusions:

(1) The greatest joint opening usually occurs at the crown section or quarter section of the dam, especially when the lowest vibration mode is not symmetrical.

(2) As the deformation of the abutment block is restricted by the canyon wall, the joints adjacent to the abutment block or its neighbor have the most slippage in the radial direction. This phenomenon becomes particularly noticeable for the U-shaped canyon. The joint opening in the normal direction may also have a very large value.

(3) The joint opening dramatically reduces the arch tensile stresses, particularly in the center part of the dam, but it does not have a significant effect on the cantilever stresses since the arch action is still provided by the shear keys. Distribution of the minor principle stresses (compression) over the dam body for cases with and without joint opening is very similar. Discontinuity of stress contours takes place when they cross the joints.

(4) The tendency for joint slippage in the tangential direction during strong earthquakes may cause damage to shear keys and waterstops. The strength of the shear keys to resist strong earthquake action must be checked.

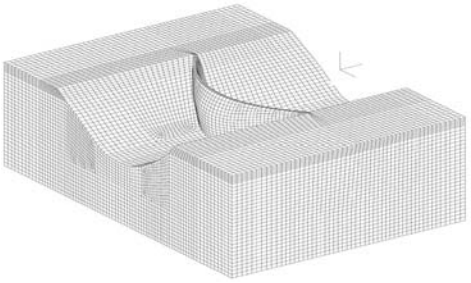

Fig. 10 FEM model of Xiaowan arch dam

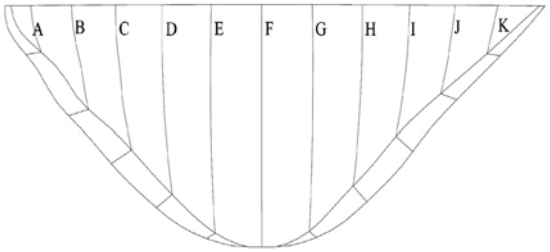

Fig. 11 Joint arrangement of Xiaowan arch dam

Table 8 Comparison of maximum joint opening in normal direction

cm

Case		A	B	C	D	E	F	G	H	I	J	K
3 joints	U			0.6849			1.2259			1.2951		
	D			1.1347			1.8848			1.1774		
5 joints	U		1.5867		0.3287		1.1062		0.8633		2.3172	
	D		1.607		0.3203		1.7771		0.6702		2.5027	
9 joints	U		1.3829	0.4310	0.4516	0.4585	0.9584	0.5355	0.8793	0.7608	1.4822	
	D		1.2565	0.3001	0.4137	0.5134	1.5062	0.9627	0.7865	0.7913	1.3519	
11 joints	U	0.8575	1.0061	0.4683	0.4613	0.4036	1.0395	0.6000	0.8586	0.7193	1.1736	1.0217
	D	0.9141	0.8925	0.3207	0.4230	0.3705	1.6136	1.102	0.7678	0.7415	1.0592	1.0752
5 joints*	U		1.853		0.273		0.973		0.485		2.738	
	D		1.843		0.011		1.748		0.371		2.789	

Table 9 Comparison of maximum joint sliding in tangential direction

cm

Case		A	B	C	D	E	F	G	H	I	J	K
3 joints	U			4.7311			3.1997			4.7885		
	D			4.6501			3.3892			4.8248		
5 joints	U		6.2663		2.1619		2.2786		2.5415		7.4648	
	D		5.8047		2.2906		2.4583		2.6318		6.49	
9 joints	U		7.0304	1.4239	2.1980	2.3683	1.9228	3.4715	1.738	1.7326	5.5158	
	D		6.5342	1.4777	2.3464	2.5459	2.0925	3.7378	1.804	1.671	4.6594	
11 joints	U	2.4832	6.4028	1.7103	2.1805	2.2209	1.9859	3.4883	1.740	1.7542	5.4308	2.3265
	D	2.138	6.9595	1.7675	2.3211	2.4017	2.1565	3.7812	1.8068	1.709	5.0276	2.1505

5 Modeling of dam-foundation interaction

The problems of dam-foundation interaction have been studied by many researchers. This investigation emphasizes the effects of the variation of foundation stiffness and foundation inhomogeneity on the seismic response of the dam.

The scaled boundary finite element method (SBFE) presented by Song and Wolf (1997) is employed in this study. This approach has the advantages that the radiation condition for the unbounded medium is satisfied exactly and general material anisotropy can be analyzed without increasing the computational effort. In addition, the discretization is only conducted on the structure-foundation interface, reducing the spatial dimension by one.

The 103 m high Koyna dam is used to study the dam-foundation interaction effects and the Koyna earthquake record in the horizontal direction with maximum acceleration 0.3 g is used as the input ground motion.

Material constants of the dam are assumed as: modulus of elasticity E=30 GPa, Poisson's ratio v=0.20 and mass density ρ=2500 kg/m^3. The following cases have been studied (Du and Lin, 2005): (1) the ratio of foundation modulus to dam modulus equals $a=E_f/E_d$=0.5, 1.0, 2.0 and 3.0 respectively; (2) rigid foundation $E_f=\infty$;(3) massless foundation; (4) inhomogeneous foundation, where the modulus of elasticity of foundation material varies as a power function of the depth $E_f(r)=E_0(r/r_0)^g$, with the value of exponent g equal to 0.0, 0.5, and 1.0, respectively. The inhomogeneous foundation is usually assumed to be a layered distribution as shown in Fig.12(a), and the simulated foundation by the SBFE approach is shown in Fig.12(b). According to Meek and Wolf (1993), the conical part of the foundation beneath the interface of the structure plays a dominant role in the dynamic interaction, and the influence of such difference of foundation inhomogeneity is insignificant.

The calculated results of the response of the dam crest expressed as the dynamic amplification factor for different foundation cases are demonstrated in Fig.13, the contours of the maximum tensile stresses for three foundation cases is shown in Fig. 14, and the maximum earthquake stresses calculated by different models for points *A*, *B*, *C* (shown in Fig.14) are given in Table 10. The parameter f_1 corresponds to the first frequency of the dam-reservoir-foundation system for a=1.0, when the dynamic dam-foundation interaction effect is included.

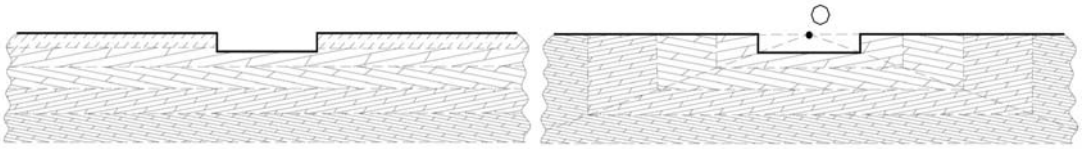

(a) Layered (b)Simulated

Fig. 12 Anisotropic foundation

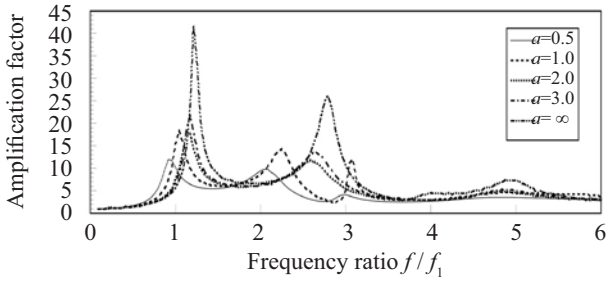

(a) For 5 cases of foundation stiffness (dynamic interaction effect included)

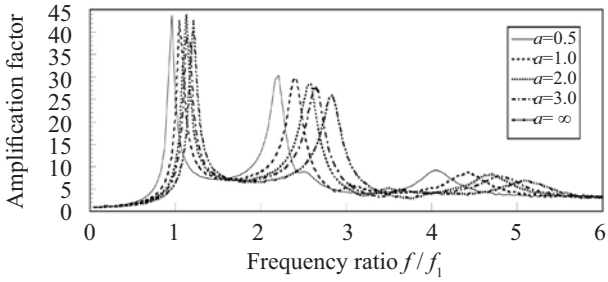

(b) For 5 cases of foundation stiffness (massless foundation)

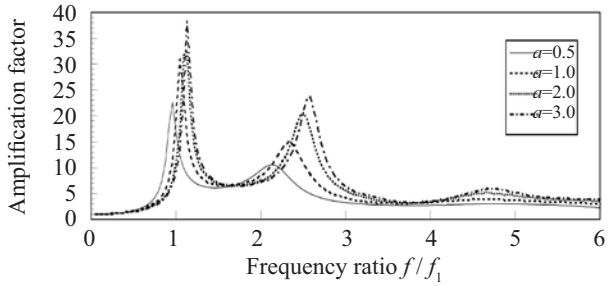

(c) For inhomogeneous foundation g=0.5 (dynamic interaction effect included)

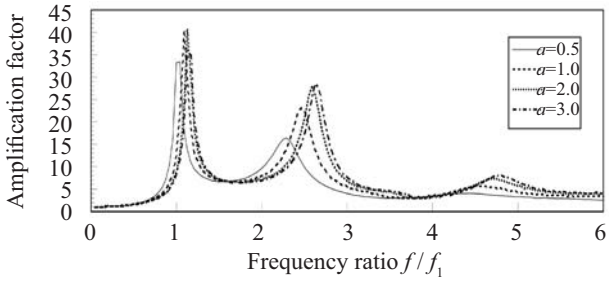

(d) For 5 cases of foundation stiffness g=1.0 (massless foundation)

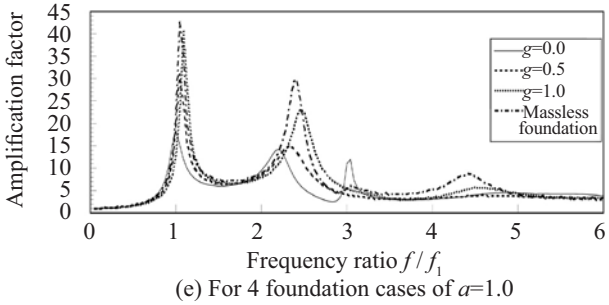

(e) For 4 foundation cases of a=1.0

Fig. 13 Complex frequency response of dam crest for different foundation cases

Dam-unbounded foundation interaction effects have also been studied for a 210m high Dagangshan arch dam. Material constants for the study are assigned as: for the dam body E_d=3.12×10^4 MPa, ν_d=0.17, ρ_d=2.4×10^3 kg/m^3; and for the foundation rock E_0=1.6×10^4 MPa, ν_0=0.245, ρ_0=2.6×10^3 kg/m^3.

The dam and the near field is treated as a substructure shown in Fig. 15(a) and partitioned for SBFE analysis. Each sub-region has its own scaling center, and the model of the far field unbounded foundation is shown in Fig. 15(b).

Three cases have been calculated and compared, namely (a) inhomogeneous foundation stiffness E_f, which varies as an exponential function along the depth r, $E_f(r)=E_0(r/r_0)^g$; (b) homogeneous foundation; and (c) massless foundation.

The frequency response functions at the central point of the dam crest for these cases are shown in Fig.16. In order to achieve a better understanding of the effect of near-field stiffness on the arch dam-foundation interaction, the frequency response function for three cases of near-field foundation stiffness: $E=E_f$, $E=2E_f$ and $E=0.5E_f$ have also been evaluated by the SBFE analyses and shown in Fig.17. The maximum stresses on the arch dam subjected to the Koyna earthquake shocks are given in Table 11.

The results regarding the dam-foundation interaction effects are summarized as follows:

(1) In comparison with the massless foundation, the dam-foundation interaction reduces the resonant

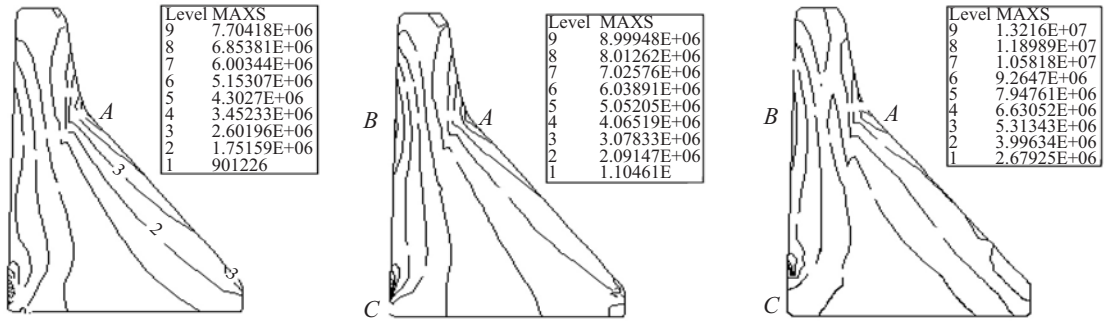

(a) Dam-foundation interaction (b) Rigid foundatio (c)Massless foundation

Fig. 14 Maximum tensile stress response of Koyna dam for three foundation cases (MPa)

Table 10 Maximum earthquake stresses of Koyna dam subjected to the Koyna wave

Cases studied	a=0.5 g=0.0	a=1.0 g=0.0	a=2.0 g=0.0	a=3.0 g=0.0	a=1.0 g=0.5	a=1.0 g=1.0	a=∞ (Rigid foundation)	a=1.0 (Massless foundation)
Max. tension at point *A*	5.91	8.55	9.66	10.1	10.5	10.9	9.99	15.1
Max. compression at point *A*	-5.93	-7.00	-8.33	-9.24	-9.08	-10.4	-11.9	-15.7
Max. tension at point *B*	5.23	5.66	6.44	6.90	7.40	9.43	6.20	12.1
Max. compression at point *B*	-3.17	-4.88	-5.26	-5.51	-6.81	-7.85	-7.79	-11.9
Max. tension at point *C*	2.25	3.47	3.83	4.07	4.85	5.72	5.33	9.57
Max. compression at point *C*	-3.75	-4.11	-4.42	-4.75	-5.08	-6.51	4.41	-8.58

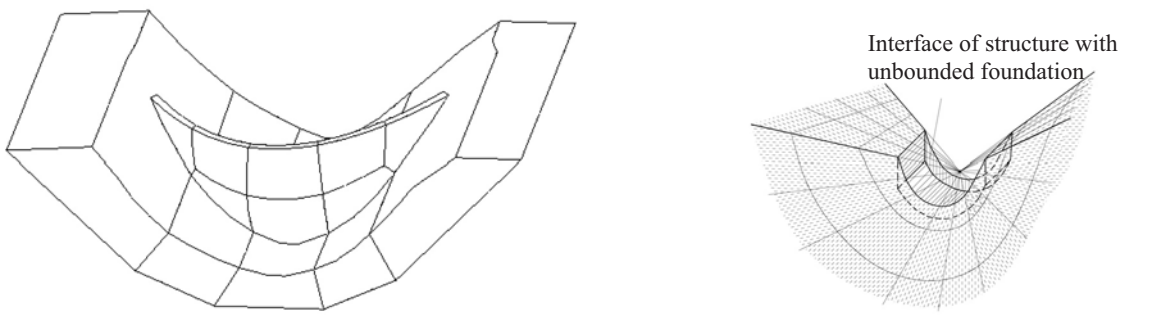

(a) Partitioning dam and near foundation (b) Partitioning unbounded far-field foundation

Fig. 15 Model of dam and foundation for SBFE analyses

peaks, especially the high resonant peaks, and widens the frequency bandwidth. As a result, the earthquake response of the dam is greatly reduced.

(2) The interaction effects, including the effect of foundation inhomogeneity, are more noticeable in the massive gravity dams, while they are less significant for the slender arch dams.

(3) Taking into consideration the interaction effects, the amplitude of resonant response peaks are sensitive to the variation of foundation stiffness. However, in the massless foundation model, these resonant peaks hardly change as the foundation stiffness changes.

(4) The massless foundation model gives an over-conservative estimation of the seismic response. This agrees with the conclusion of Proulx *et al*. (2004). They have conducted in-situ forced- and ambient-vibration tests and field observation of the earthquake response of three large arch dams. They found that when using the massless foundation approach, the calculated response is too large when compared with the observed response.

6 Nonlinear modeling of concrete behavior

To ascertain the amount of damage to and stability of a dam during strong earthquakes, nonlinear modeling of concrete is an important research need.

Work on this subject is under way, and two types of models and algorithms have been developed and presented in the literature. One uses concepts from fracture mechanics to model the discrete cracking due to earthquake excitation. In cases when the finite element method is implemented, the domain must be remeshed as

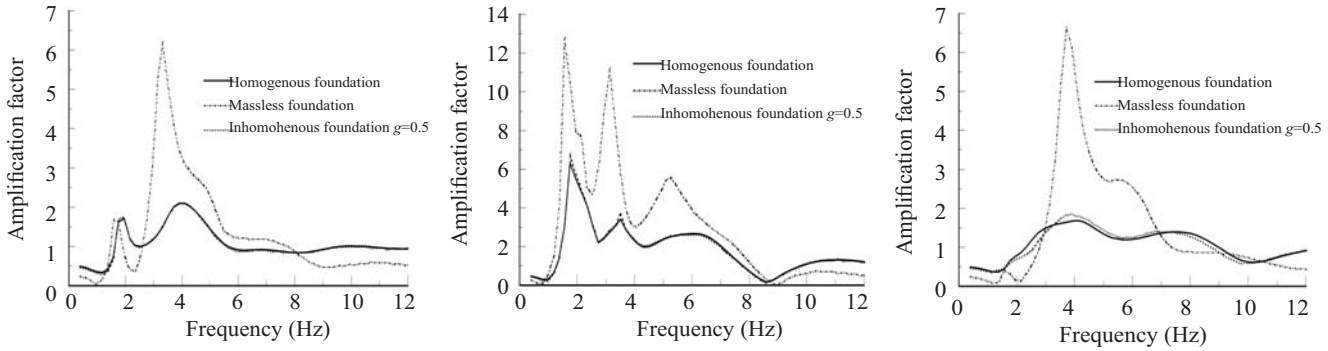

(a)Excitation in river direction (b) Excitation in cross-river direction (c) Excitation in vertical direction

Fig. 16 Complex frequency response of arch dam-foundation system for three cases of foundation model

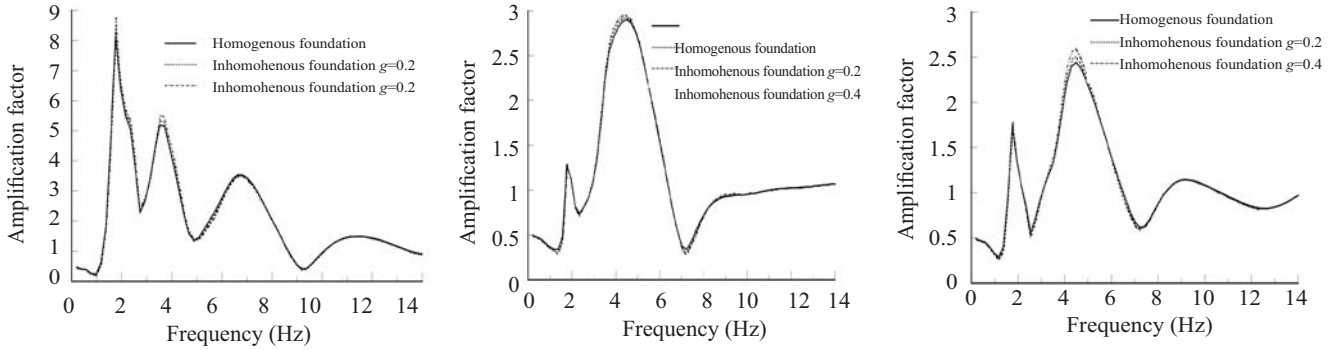

(a) Component of response in the river direction (b) Component of response in the cross-river direction (c) Component of response in the vertical direction

Fig. 17 Complex frequency response of arch dam-foundation system for three cases of near-field stiffness

Table 11 Maximum earthquake stress of Dagangshan arch dam for different cases of near-field foundation stiffness

		Homogenous unbounded foundation			Massless foundation		
		$E=E_f$	$E=2E_f$	$E=0.5E_f$	$E=E_f$	$E=2E_f$	$E=0.5E_f$
Upstream face	Max. tension	8.2	9.4	7.9	12.1	14.0	18.3
	Max. compression	-8.1	-8.7	-7.5	-12.0	-14.2	-17.9
Downstream face	Max. tension	7.1	7.9	6.9	12.1	13.7	15.6
	Max. compression	-7.1	-8.3	-6.6	-12.0	-13.8	-16.8

the crack surface changes. In addition, mesh objectivity must be ensured by certain techniques. The other type uses continuum models because they can be easily implemented using standard finite element analysis procedures. The smeared crack model was first applied, and in spite of many improvements, this approach is still difficult to define rigorous evolution rules for a failure surface under multi-axial cyclic loading conditions. In contrast to the smeared crack approach, the continuum damage mechanics approach was developed by researchers. Concrete exhibits strong strain-softening behavior in the post-failure range, showing a significant elastoplastic coupling of the degradation of the elastic modulus with increasing plastic deformation. A damage mechanics model is combined with a plasticity model to form the elastic-plastic-damage model to adequately describe the main characteristics of concrete structures. The nonlinear modeling of concrete is still under development. Moreover, most of the models developed and algorithms described in the literature were only designed to account for two-dimensional problems. Further research is needed to develop realistic applicative models that are rational, reliable and practical and can be directly implemented into a general purpose finite element analysis with relative ease.

Some results of the damage mechanics approach developed by the authors (Yan and Lin, 2005) are given in the following examples.

Figure 18 demonstrates the contours of the damage evolution of the Koyna Dam subjected to the Koyna wave excitation. Figure 19 shows the envelope values of the damage factors of the Dagangshan arch dam subjected to the Koyna earthquake ground motions.

7 Conclusions

Some of the problems that are considered to be important with regard to the safety of concrete dams

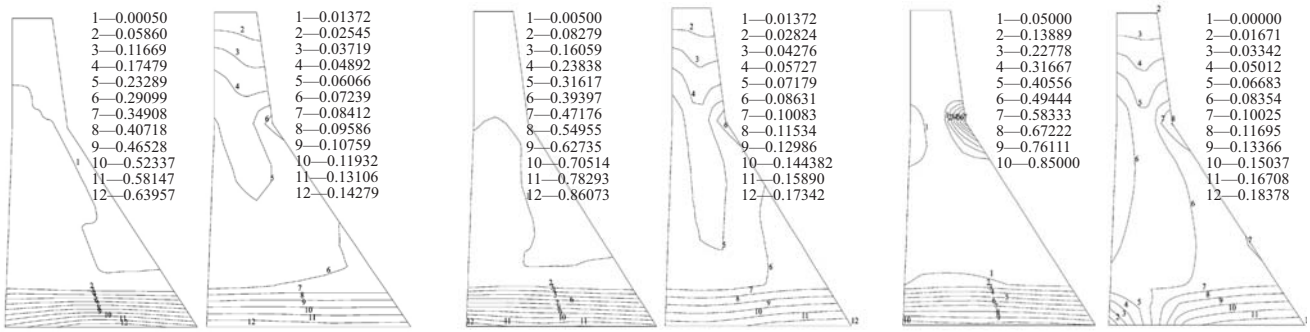

(a) t=0.94s (b) t=2.12s (c) t=2.50s

Fig. 18 Contours of damage evolution of Koyna Dam

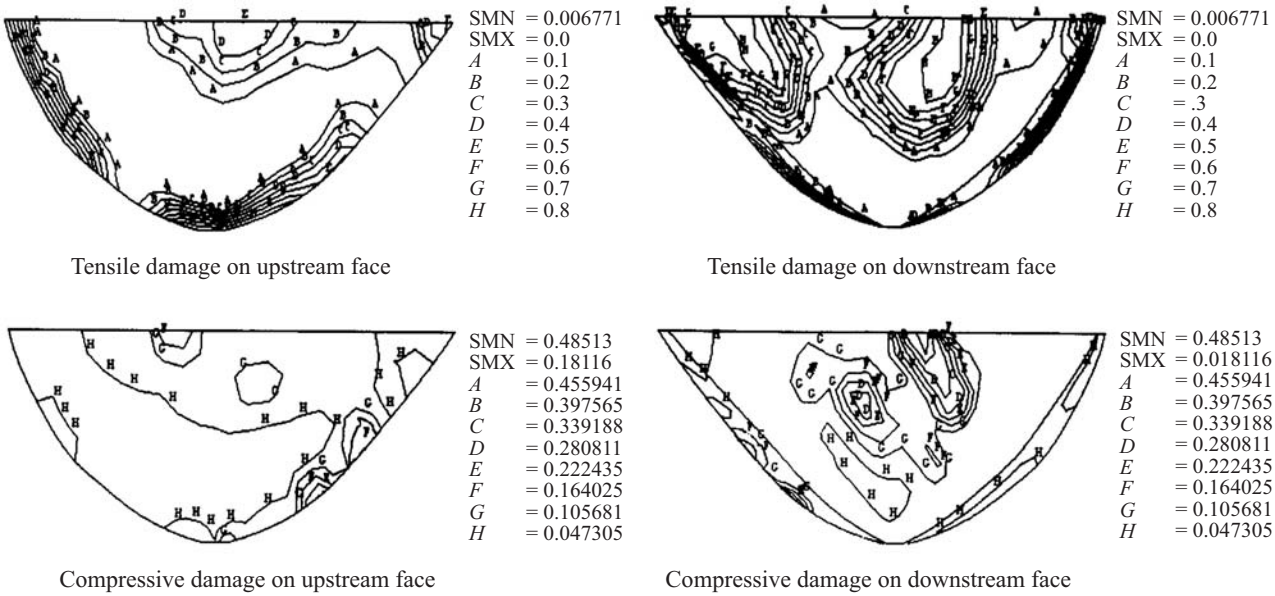

Fig. 19 Isograms of damage factors of Dagangshan arch dam subjected to Koyna earthquake shock

against strong earthquake shocks have been studied. Based on this research, the following conclusions can be drawn:

(1) Strain-rate effects become noticeable in the inelastic range, and should be taken into consideration in the earthquake safety assessment of concrete dams.

(2) Joint opening effects reduce the tensile stresses in the majority part of an arch dam. The integrity of the dam can be ensured by the shear keys, provided they have enough strength to resist the large shear forces which occur during strong earthquakes.

(3) Dynamic dam-foundation interaction effects tend to reduce the maximum seismic response of the dams. The inhomogeneity of the foundation material greatly affects the seismic response of gravity dams, and becomes less significant for more slender arch dams. The massless foundation approach overestimates the seismic response of the dam.

(4) To assess the earthquake safety of concrete dams during strong earthquakes, nonlinear modeling of concrete is an important research need. This problem is still under development. Various models and algorithms currently available could be helpful to better understand the damage evolution of concrete dams during strong earthquakes. Further improvement to the models for implementation into practical design applications is necessary.

Acknowledgements

This research is sponsored by the National Natural Science Foundation of China under grant No. 50139010. Grateful appreciation is also expressed to the author s students, Dr. Shi-yun Xiao, Dr. Jian-bo Li and Doctoral candidates Mr. Dong-ming Yan and Mr. Jian-guo Du, who have taken part in this research.

References

Bischoff PH and Perry SH (1991), "Compressive Behavior of Concrete at High Strain Rates," *Materials and Structures*, **24**: 425-450.

Du JG and Lin G (2005), "Effect of Foundation Stiffness and Anisotropy on the Seismic Response of Concrete Dams," *Chinese Journal of Geotechnical Engineering*, **27**(7): 819-823. (in Chinese)

Du XL, Tu J and Chen HQ (2000), "Non-linear Seismic Response of Arch Dam-foundation Systems with Cracked Surface," *Earthquake Engineering and Engineering Vibration*, **20**: 11-20. (in Chinese)

Du Xiuli and Wang Jinting (2004), "Seismic Response Analysis of Arch Dam-water-rock Foundation Sytems," *Earthquake Engineering and Engineering Vibration*, **3**(2):283-291

Fenves GL, Mojtahedi S and Reimer RB (1992), "Effect of Contraction Joints on Earthquake Response of an Arch Dam," *Journal of Structural Engineering*, ASCE, **118**(4): 1039-1055.

Hall JF (1998), "Efficient Non-Linear Seismic Analysis of Arch Dams," *Earthquake Engineering and Structural Dynamics*, **27**: 1425-1444.

Lin G and Xiao SY (2002), "Seismic Response of Arch Dams Including Strain-rate Effects," *Proceedings of the International Conference on Advance and New Challenges in Earthquake Engineering Research*, Ko JM, Xu YL , Editiors, Harbin and Hong Kong, pp.331-338.

Lin G, Chen JY and Xiao SY (2003), "Dynamic Behavior of Concrete and Nonlinear Seismic Response of Arch Dam," *Chinese Journal of Hydraulic Engineering*, (6): 30-36. (in Chinese)

Lin G, Hu ZQ and Chen JY (2004), "Dynamic Analysis of an Arch Dam Including Joint Opening Effects," *Earthquake Engineering and Engineering Vibration*, **24**(6): 45-52. (in Chinese).

Liu Xinjia, Xu Yanjie, Wang Guanglun and Zhang Chuhan (2002), "Seismic Response of Arch Dams Considering Infinite Radiation Damping and Joint Opening Effects," *Earthquake Engineering and Engineering Vibration*, **1**(1):65-73.

Malvar LJ and Ross CA (1998), "Review of Strain Rate Effects for Concrete in Tension," *ACI Materials Journal*, **95**(6): 735-739.

Meek JW and Wolf JP (1993), "Why Cone Models Can Represent the Elastic Halfspace," *Earthquake Engineering and Structural Dynamic*, **22**: 759-771

Proulx J, Darbre GR and Kamileris N (2004), "Analytical and Experimental Investigation of Damping in Arch Dams Based on Recorded Earthquakes," *13th World Conference on Earthquake Engineering*, pp.68, Vancouver, Canada, Aug.1-6.

Song CM and Wolf JP (1997), "The Scaled Boundary Finite-element Method Alias Consistent Infinitesimal Finite-element Cell Method- for Elastodynamics," *Computer Methods in Applied Mechanics and Engineering*, **147**: 329-355.

Valliappan S. Yazdchi M and Khalili N (1999), "Seismic Analysis of Arch Dam A Continuum Damage Mechnics Approach," *International Journal of Numerical Methods in Engineering*, **45**: 1695-1724.

Yan DM, Lin G and Wang Z (2005), "Study on the Uniaxial Tensile Properties of Concrete Under Variable-Amplitude Cyclic Loading," *Chinese Journal of Hydraulic Engineering*, **36**(5): 593-597. (in Chinese)

Yan XR and Lin G (2005), "An Anisotropic Damage Model of Concrete Based on Material Stress-strain Relationship and Its Application," *Water Sciences and Engineering Technology*, (4): 39-42. (in Chinese)

Zhang CH, Xu YJ, Wang GL and Jin F (2000), "Non-linear Seismic Response of Arch Dam with Contraction Joint Opening and Joint Reinforcements," *Earthquake Engineering and Structural Dynamic*, **29**: 1547-1566.